Self-, Cross-, and Induced-Phase Modulations of Ultrashort Laser Pulse Propagation

R. R. Alfano
P. P. Ho

Reprinted from
IEEE JOURNAL OF QUANTUM ELECTRONICS
Vol. 24, No. 2, February 1988

Self-, Cross-, and Induced-Phase Modulations of Ultrashort Laser Pulse Propagation

R. R. ALFANO AND P. P. HO

(*Invited Paper*)

Abstract—**Spectral broadenings of picosecond and femtosecond pulses arising from self-phase modulation, cross-phase modulation, induced-phase modulation, and induced spectral broadening in condensed matter are reviewed. The spectral broadening of the Raman line produced in an optical fiber is compared to the spectral width of the pump laser line as evidence for cross-phase modulation. Induced-phase modulation of a weak picosecond 527 nm laser pulse in BK-7 glass occurred in the presence of an intense picosecond 1054 nm laser pulse. The induced spectral broadening about a weak non-phase-matched second harmonic pulse at 527 nm is observed by propagating an intense primary 1054 nm picosecond laser pulse through ZnSe crystals. Induced spectral broadened pulses with wavelengths spanning from 500 to 570 nm generated in ZnSe were found to be emitted at nearly the same time as the 1054 nm pump pulse. The apparent dispersionless-like propagation of the induced spectrally broadened pulse is discussed.**

I. Introduction

NONLINEAR optics is an important field of science and engineering because it can generate, transmit, and control the spectrum of laser pulses in solids, liquids, gases, and fibers. When an intense laser pulse propagates through such materials, it changes the refractive index. This in turn changes the phase, amplitude, and frequency of the incident laser pulse. A phase change can cause a frequency sweep within the pulse envelope. This process is called *self-phase modulation* (SPM) [1]–[25]. Photons at the laser frequency can also parametrically generate photons at Stokes and anti-Stokes frequencies in an angular pattern due to the required phase-matching condition. The four-photon parametric generation (FPPG) process usually occurs together with the SPM process.

When two laser pulses of different wavelengths propagate simultaneously in a condensed medium, coupled interactions (cross modulation and gain) occur through the nonlinear susceptibility coefficients. These coupled interactions of two different wavelengths can introduce phase modulation [26], [27], amplitude modulation, and spectral broadening [27] in each pulse due to the other pulse. An example of a coupled interaction is the optical Kerr effect. We will discuss three recent observations of spectral broadening arising from the coupled interaction of two laser pulses with different wavelengths. These processes have been termed cross-phase modulation, induced-phase modulation, and induced spectral broadening. Each process has a particular signature.

When a coherent vibrational mode is excited by a laser, stimulated Raman scattering (SRS) occurs. SRS is an important process which competes with and can couple with SPM [27]–[30]. The interference between SRS and SPM, which causes the change of the emission spectrum and the phase modulation of pulse envelopes, is called *cross-phase modulation* (XPM) [27]. The Stokes pulse broadens due to a combination of XPM and Raman parametric amplification. The spectral broadening measured about the SRS wavelengths in liquids and recently in glass fibers [28] originates from both SPM and XPM processes.

Another important spectrally broadened process similar to XPM is called *induced-phase modulation* (IPM) [31], [32]. The experimental arrangement of this process is similar to the optical Kerr effect; namely, a weak pulse at a different frequency propagates through a disrupted medium whose index of refraction is changed by an intense laser pulse. The phase of the weak optical field can be modulated by the time variation of the index of refraction originating from the primary intense pulse. Both the weak and strong pulses are produced outside the medium and can be controlled by the researcher.

Most recently, the *induced spectral broadening* (ISB) [33], [34] process of a weak *non-phase-matched* second harmonic (SH) pulse was produced inside a nonlinear medium to the propagation of a primary picosecond laser pulse through ZnSe crystals. The ISB pulse spread from 500 to 570 nm was found to travel at nearly the same speed as the pump pulse at 1054 nm in ZnSe. ISB is a combination of non-phase-matched SHG and XPM interfering in the time domain.

The spectral broadening of picosecond and femtosecond laser pulses in condensed matter due to SPM covers a frequency band up to 10 000 cm^{-1} from UV to IR with picosecond to femtosecond pulse durations [22], [35]. Over the years, this ultrafast supercontinuum pulse source has been applied to time-resolved absorption spectroscopy [34], nonlinear optical effects [36], [37], pulse compression [18], [38], [39], squeeze states [40], and fi-

Manuscript received May 18, 1987; revised August 7, 1987. This work was supported in part by the U.S. Air Force Office of Scientific Research under Grant AFOSR 86-0031, in part by the National Science Foundation under Grant NSF-OIR 84-13144, and in part by Hamamatsu Photonics K. K.

The authors are with the Institute for Ultrafast Spectroscopy and Lasers and the Photonics Application Laboratory, Departments of Electrical Engineering and Physics, The City College of New York, New York, NY 10031.

IEEE Log Number 8717797.

TABLE I
BRIEF HISTORY OF EXPERIMENTAL CONTINUUM GENERATION

Investigator	Year	Material	Wavelength, Laser/Pulsewidth	Spectral	Frequency Shift	Process
Alfano and Shapiro	1969–1973	Liquids and solids	530 nm/8 ps or 1060 nm/8 ps	Visible Near IR	10 000 cm^{-1}	SPM
Stolen	1974–1976	Fibers	530 nm/ns	Visible	500 cm^{-1}	SPM
Shank, Fork, *et al.*	1983	Glycerol	620 nm/100 fs	UV, visible, near IR	10 000 cm^{-1}	SPM
Corkum, Ho, and Alfano	1985	Semiconductor dielectrics	10 μm/6 ps	IR	1000 cm^{-1}	SPM
Corkum and Sorokin	1986	Gases	600 nm/2 ps 300 nm/0.5 ps	Visible UV	5000 cm^{-1}	SPM
Alfano, Ho, Manassah, and Jimbo	1986	Glass	1060 nm/530 nm 8 ps	Visible	1000 cm^{-1}	IPM
Alfano, Ho, Wang, and Jimbo	1986	ZnSe	1060 nm 8 ps	Visible	1000 cm^{-1}	ISB
Alfano, Ho, and Baldeck	1987	Fibers	530 nm 30 ps	Visible	1000 cm^{-1}	XPM

ber diagnostics [15]. The frequency-broadened pulses can play an important role in ranging, imaging, remote sensing, communications, and other fields [41]. It is a key process behind the generation of 6 fs laser pulses. The newly observed ISB due to IPM has important features for communications and signal processing by allowing pulse coding in different frequency regions. Furthermore, SPM, XPM, and IPM in optical fibers could be a source of noise on signals due to interference in multiband communications and signal processing applications [42].

In this paper, we will review, discuss, and compare SPM, XPM, IPM, and ISB spectral broadening of ultrashort laser pulses in condensed matter. In all these cases, χ^3 is responsible for the modulation and spectral broadening processes. Over the past 17 years, Alfano and his coworkers were the first to observe SPM, XPM, IPM, and ISB in condensed matter and fibers using ultrashort pulses.

Table I presents major observations of the spectral broadening in different states of matter. Different types of nonlinear optical processes responsible for continuum generation arising from various susceptibility coefficients in condensed matter are given in Table II. Underlying mechanisms giving rise to these processes will not be discussed in detail here, but the electronic process is still believed to be the most important [1], [11] in the femtosecond and picosecond time scales. The bracket indicates the laser pulse intensity at a given frequency. In the SPM process, the spectral broadening of pulses involves only one principal wavelength. In an example of the XPM process, the principal wavelength generates a Stokes Raman line, and its width is broadened through the coupling of the laser pulse and the generated Raman pulse via phase changes. In the IPM process, strong and weak laser pulses at different wavelengths are generated outside the interaction material. Then these pulses enter the sample to induce additional spectral broadening of the weak pulse. There are experimental differences between XPM and IPM processes. The temporal shape of IPM is externally produced, while the Raman pulse in XPM starts from the noise level. Also, there is a definite energy transfer involved in the XPM process from the primary pulse to the Raman pulse due to the Raman gain factor. There is little energy enhancement of the weak pulse in IPM; just a modulation of phase occurs in the first-order approximation. In the ISB process, similarly to XPM and IPM, an intense laser pulse is passed into a medium. A non-phase-matched SH is generated inside the sample, becoming spectrally broadened from its interaction with the primary pulse. This is similar to XPM with the SHG pulse replacing the Raman pulse. However, ISB was found to have a unique dispersionless-like propagation property.

TABLE II
TYPES OF SPECTRAL BROADENING FROM PHASE MODULATION PROCESSES

	Input	Coupling	Output	Process
SPM	$[\omega_1]$	$\xrightarrow{\chi^3}$	$[\omega_1 \pm \Delta\omega_1]$	SPM
XPM	$[\omega_1]$	$\xrightarrow{\chi^3}$	$[\omega_1 \pm \Delta\omega_1]$	SPM
		$\xrightarrow{\chi^R}$	$[\omega_1 - \sigma \pm \Delta\omega_R]$ where $\Delta\omega_R \sim 2\Delta\omega_1$	XPM
IPM	$[\omega_1]$	$\xrightarrow{\chi^3}$	$[\omega_1 \pm \Delta\omega_1]$	SPM
	$[\omega_2]$ weak	$\xrightarrow{\chi^3}$	$[\omega_2 + \Delta\omega_2]$ where $\Delta\omega_1 \gg \Delta\omega_2$	SPM
	$[\omega_1] + [\omega_2]$	$\xrightarrow{\chi^3}$	$[\omega_1 \pm \Delta\omega_1] + [\omega_2 \pm \Delta\omega]$ where $\Delta\omega \gg \Delta\omega_2$	SPM IPM
ISB	$[\omega_1]$	$\xrightarrow{\chi^3}$	$[\omega_1 \pm \Delta\omega_1]$	SPM
		$\xrightarrow{\chi^2}$	$[2\omega_1]$	SHG
		$\xrightarrow{\chi^2, \chi^3}$	$[2\omega_1 \pm \Delta\omega_0]$ where $\Delta\omega_0 \sim 1{,}000\ cm^{-1}$.	ISB

II. EXPERIMENTAL ARRANGEMENT

A typical experimental arrangement which is used to produce and measure the spectral and temporal profiles of the spectrally broadened pulse is displayed in Fig. 1. Picosecond and femtosecond laser pump pulses are generated from mode-locked laser systems. SH pulses are often used as either the pump or the probe beams for conve-

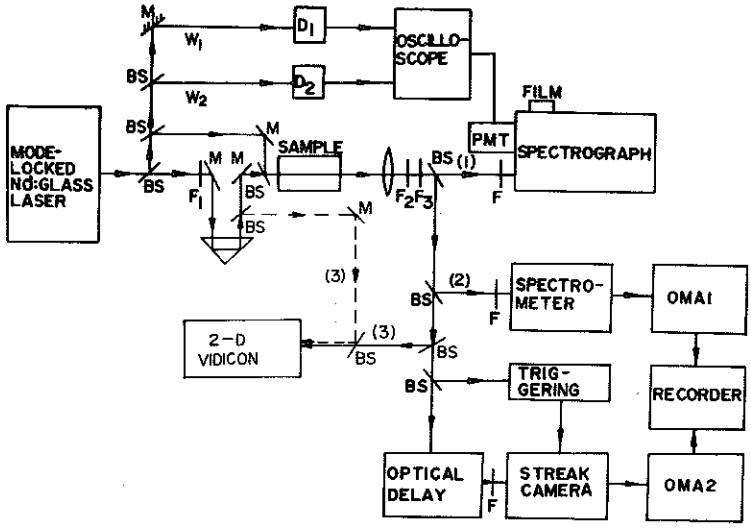

Fig. 1. Experimental setup to measure temporal and spectral profiles of ultrashort laser pulse propagating through condensed media.

nience. The pump beam is usually weakly focused into the sample. The output signals are passed through filters to remove the incident laser pulses and separated into three paths for diagnosis. Along path 1, the beam is imaged onto the slit of a 0.5 m Jarrell-Ash spectrograph to separate the spectral contributions arising from possibly different mechanisms of the supercontinuum generation. By analyzing the spatial and angular distribution of the spectrum, one can separate the phase modulation from FPPG processes. In spectral measurements, photographic films or multichannel photodetectors are used to measure the spatial distribution of the emission supercontinuum spectrum. Photomultipliers are used to obtain quantitative readings. To distinguish different contributions from either the phase modulation or FPPG, geometrical blocks are arranged in the path for the selection of a particular process. The beam along path 2 is directed into a spectrometer with an optical multichannel analyzer to measure the supercontinuum spectral intensity distribution. The spectrum is digitized, displayed, and stored in 500 channels as a function of wavelength. The beam along path 3 is delayed and directed into a 2 ps Hamamatsu model #C1587 streak camera [43] to measure the temporal distribution of the laser pulses and the spectrally broadened pulse.

The spectral broadening of ultrashort laser pulses arising from *SPM*, *XPM*, *IPM*, and *ISB* will be described in Sections III–VI.

III. SPM

When an optical electromagnetic field propagating in a medium satisfies Maxwell's equations, the wave equation can be expressed as

$$\vec{\nabla} \times \vec{\nabla} \times \vec{E} + 1/c^2\, \partial^2 \vec{E}/\partial t^2 = -4\pi/c^2\, \partial^2 \vec{P}/\partial t^2, \quad (1)$$

the polarization density is given by a linear and nonlinear part:

$$\vec{P} = \vec{P}^{\mathrm{L}} + \vec{P}^{\mathrm{NL}} \quad (2)$$

and the linear part of the polarization is related to the susceptibility through

$$\vec{P}^{\mathrm{L}}(\vec{x}, w) = \chi(w)\, \vec{E}(\vec{x}, w). \quad (3)$$

We are interested in the propagation of a nearly monochromatic pulse of light for which the amplitude E is given by

$$\vec{E} = \mathrm{Re}\left\{\vec{E}(\vec{x}, t)\, e^{-iw_0 t} e^{ik_0 z}\right\} \quad (4)$$

and E varies little in a period $2\pi/w_0$. The instantaneous phase of the light wave is given by

$$\phi(t) = w_{\mathrm{L}} t - n(t) w_{\mathrm{L}} z/c. \quad (5)$$

The simplest of all forms of nonlinear polarization density responsible for SPM is given by

$$P_j^{\mathrm{NL}} = \eta \left|E\right|^2 E_j \quad (6)$$

where η is a proportionality constant. Equation (6) is a special case of the general third-order nonlinear polarization

$$P_j^{\mathrm{NL}} = D\chi^3_{jklm}(-w_4, w_1, w_2, w_3) \cdot E_k(w_1)\, E_l(w_2)\, E_m(w_3). \quad (7)$$

The index of refraction change for such a nonlinearity is

$$\delta n = 2\pi\eta/n \left|E\right|^2 = \tfrac{1}{2} n_2 \left|E\right|^2. \quad (8)$$

Fig. 2 displays the salient features of SPM. Having determined δn, the electric field in w space can be evaluated using the method of stationary phase. Critical points are located at

$$w - w_{\mathrm{L}} = -w_{\mathrm{L}}(z/c)\, \partial/\partial t\, (\delta n). \quad (9)$$

Assuming δn to be a bell-shaped curve, t_1 and t_2 to be its inflection points, and t' and t'' to be the solutions of the critical points equation, the maximum frequency broadening of Stokes and anti-Stokes occurs at t_1 and t_2. After

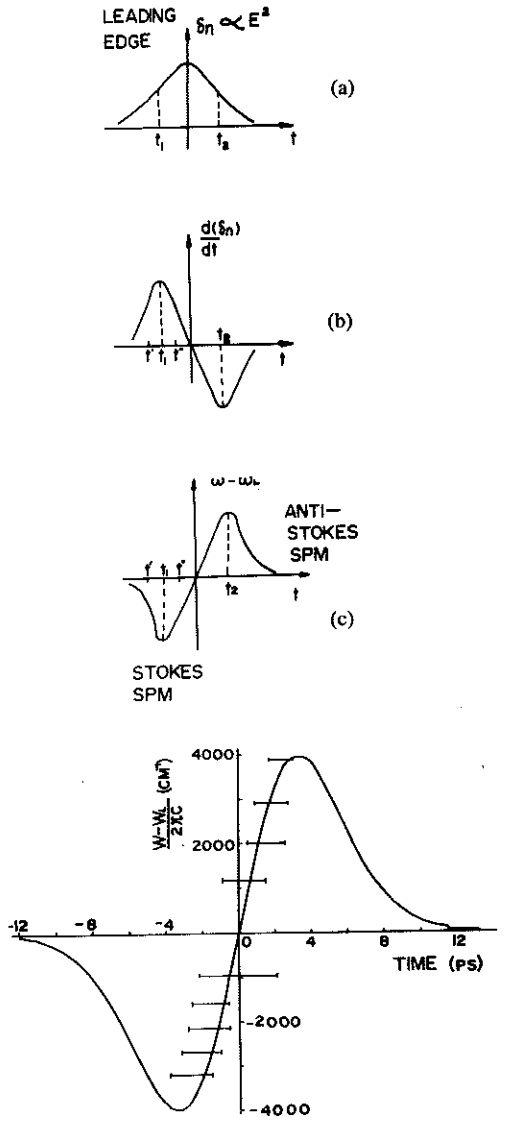

Fig. 2. A theoretical model of the frequency generation within a Gaussian pulse envelope by the SPM process. (a) Index of refraction change as a function of time. (b) Time derivative of the refractive index change. (c) Frequency broadening as a function of time. (d) Measured temporal distribution of supercontinuum [44] with a SPM mode [1] using an 8 ps Gaussian laser pulse. The horizontal axis is the time in picoseconds. The vertical axis is the frequency shift of the supercontinuum as a function of pulse time profile. The solid line was calculated from (9) by assuming $\omega_0 n_2 l/c \sim 3.6\ \mathrm{TW/cm^2}$.

Fourier transformation, the spectral intensity is given by

$$S(w) = c/4\pi \left| E(w) \right|^2. \qquad (10)$$

Fig. 2 indicates that the frequency extent is inversely proportional to the pulse duration. The Stokes broadened pulse is leading the anti-Stokes broadened pulse within the generation of the incident pulse envelope. The maximum frequency extent from this analysis can be expressed as

$$\left| \Delta\omega \right| \sim \omega_0 n_2 E_0^2 z / \left[(2\pi \ln 2)^{0.5} c\tau \right] \qquad (11)$$

where τ is the pulse duration of the incident laser. From the above simple analysis for SPM, the spectrum of the supercontinuum produced by a 100 fs laser pulse spans from 0.19 to 1.6 μm [22], [35], [38] by 8 ps glass lasers, which span from 0.5 to 1.5 μm [1], and by a 3 ps CO_2 laser pulse 3–14 μm [14].

A. Experimental Evidence of SPM

In 1970, Alfano and Shapiro [1] first observed supercontinua spread over 10 000 $\mathrm{cm^{-1}}$ in liquids, glasses, and crystals. Spectral broadenings which evolved through and beyond the electronic absorptions were demonstrated by Alfano *et al.* [12] using a picosecond laser pulse generated near electronic resonances in PrF_3 crystals in 1974. Shank *et al.* [39] observed the supercontinuum in CS_2-filled fibers in 1974, and Stolen and Lin [15] verified the SPM process in optical fiber glasses in 1978. In 1983, Shank and his co-workers [22], [38] demonstrated the spectral distribution of SPM in a glycerol jet stream using femtosecond laser pulses. Corkum *et al.* [14] observed the SPM process spanning from 3 to 14 μm using picosecond CO_2 laser pulses in semiconductors and dielectrics in 1985. Recently, Corkum *et al.* [25] and Sorokin *et al.* [26] observed the SPM in gases using subpicosecond laser pulses in the visible and near UV, respectively. All these key observations and other numerous measurements have confirmed that SPM is one of the dominant processes responsible for the spectral broadening of ultrashort laser pulses.

1) Spectral Features:

a) Spatial Distribution of Non-Phase-Matched Spectra: Usually, the spectral emission of spectrally broadened pulses exhibits both SPM and FPPG. A typical spectrum from water is displayed in Fig. 3. The spectrally broadened pulse was generated using a collimated 8 ps 530 nm laser pulse propagating in 10 cm of water [44], [45]. The collinear part of the spectrum arising from the SPM process has nearly the same spatial distribution as the incident 530 nm laser pulse. Two emission wings correspond to FPPG emission. The phase matching of the FPPG process requires that different generated wavelengths be emitted at different angles from the incident laser beam direction. The measured far-field patterns of filaments have shown that FPPG pulses form circles with a radius which depends on angle (i.e., wavelength) at the entrance slit plane. Filaments at different z points form circles with different radii even if the wavelengths are the same and show the multiple cone structure on the slit of a spectrograph. Filaments at different radial points form circles centered at different points and have features like an interference pattern. Although SPM pulses travel collinearly with the 530 nm laser pulse, the wavefronts are not planar due to diffraction. These wavefronts from different filaments can interfere with each other, forming the modulation pattern. The formation of filaments is a stochastic process. Therefore, the resultant modulation patterns are not reproducible in bulk samples.

b) Modulated Spectra in Optical Fibers: Using a mode-locked argon-ion laser, Stolen and Lin [15] have observed a modulated broadened frequency over 100 $\mathrm{cm^{-1}}$ in width the single-mode silica core fibers. The spectrum

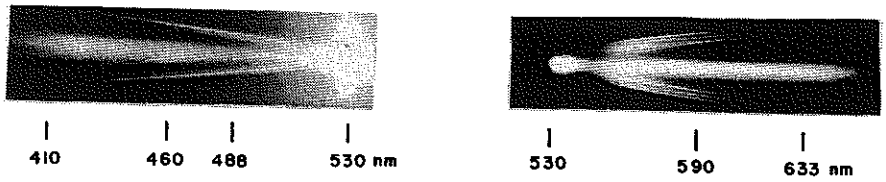

Fig. 3. Photographs of the emission spectrum of the spectrally broadened pulse in water. The horizontal signal is SPM. The angular wings are FPPG.

is in good agreement with the calculated curves based on the SPM process [1].

2) Temporal Features: Another signature of the SPM process is that the Stokes broadened frequency is generated at the leading edge of the pump pulse, and the anti-Stokes broadened frequency is generated at the trailing edge of the pump pulse when $n_2 > 0$. This is shown in Fig. 2(c). The generation of the supercontinuum in a 20 cm long CCl_4 liquid after correction for the group velocity dispersion is fitted with a calculated curve, shown in Fig. 2(d) [44]. Futhermore, using 100 fs laser pulses and an ethylene glycol thin jet stream, Shank [22], [38] *et al.* have clearly identified the spectral broadening as arising from the SPM generation process from the temporal distribution in the pulse.

B. SPM Generation and Propagation

As mentioned above, there are three major modulation processes responsible for the generation of the ultrafast supercontinuum [46]–[49]: phase modulation (SPM, XPM, and IPM), FPPG, and SRS. In the SPM process, a newly generated wavelength could have bandwidth-limited durations at a well-defined time location [22], [44] within the pulse envelope. This is, $\tau_{SPM}(\omega) \ll \tau_{laser}$. The duration of the spectrally broadened pulse from FPPG and SRS processes could be shorter than the pump pulse duration due to the higher gain about the peak of the pulse. In either case, the supercontinuum will have a shorter duration than the incident pulse duration. These pulses traveling in a condensed medium will be broadened in time due to the group velocity dispersion. The Stokes wavelengths travel ahead of the anti-Stokes wavelengths due to normal dispersion.

A model to describe the generation and propagation of the supercontinuum is next formulated based on local generation. The duration and the pulse delay of a supercontinuum generated by an 8 ps laser pulse in a 20 cm long liquid CCl_4 cell were directly measured with a 2 ps resolution streak camera. Typical data on the time delay of 10 nm bandwidth pulses centered at 530, 650, and 450 nm wavelengths of the supercontinuum without compression are displayed in Fig. 4. The absolute times of these three pulses were compared to a reference pulse traveling through air. The peak locations of 530, 650, and 450 nm are −49, −63, and −30 ps, respectively. The *salient features* displayed in Fig. 4 indicate that *the duration of all 10 nm band supercontinua are only about 6 ps, which is shorter than the incident pulse of 8 ps*; the Stokes side (650 nm) of the supercontinuum pulse travels ahead of the 530 nm pulse by 14 ps, and the anti-Stokes side (450 nm) of the supercontinuum lags the 530 nm pulse by 19 ps. *No* slow asymmetric *tail* for the Stokes or *rise* for the anti-Stokes pulses are displayed in Fig. 4. *These observations suggest local generation of supercontinua.* The time delays of the Stokes and anti-Stokes supercontinua related to the 530 nm pump pulse in accounted for by the filament formation at ~5 cm from the sample cell entrance window. The 5 cm location is calculated from data in Fig. 4 by

$$T_{530} - T_{USC} = \Delta x(1/V_{530} - 1/V_{USC}) \qquad (12)$$

where Δx is the total length of the supercontinuum traveled in CCl_4 after the generation, T_{530} and T_{USC} are the 530 nm and supercontinuum pulse peak time locations in Fig. 4, and V_{530} and V_{USC} are the group velocity of the 530 nm and supercontinuum pulses, respectively. T_{USC} has been corrected for the SPM generation process over the pump pulse envelope location [46]. For example, the time separation between 650 and 530 nm pulses in Fig. 4 is 14 ps. However, due to the SPM generation mechanism, the 650 nm supercontinuum was introduced at the 3 ps leading edge of the pump pulse. Therefore, $T_{650} = 14 - 3$ ps for the T_{USC} of (12) at $\lambda = 650$ nm.

The duration of the supercontinuum at the generation location is either limited by the bandwidth of the measurement from the SPM process or shortened by the parametric generation process. In either case, a 10 nm bandwidth supercontinuum will have a shorter duration than the indicent pulse. After being generated, each of these 10 nm bandwidth supercontinuum pulses travels through the rest of the CCl_4 liquid and is continuously generated by the incident 530 nm over a certain interaction length before these two pulses walk off. The interaction length l can be calculated from (12) by assigning $\Delta x = l$ to be the length over which the pump and the supercontinuum pulses stay spatially coincident for less than the duration [full width at half maximum (FWHM)] of the incident pump pulse, and $\tau = \tau_{530} - \tau_{650}$ is the duration of the supercontinuum pulse envelope. Using parameters $\tau_{USC} = 6$ ps, $V_{530} = c/1.4868$, and $V_{650} = c/1.4656$, the interaction length $l = 8.45$ cm is calculated. This length agrees well with the measured beam waist length of 8 cm for the pump pulse in CCl_4. The supercontinuum is not generated over the entire length of 20 cm, but only from about $z = 1$ to 9 cm (~ beam waist length of the laser in CCl_4). In addition, a pulse broadening of 0.3 ps calcu-

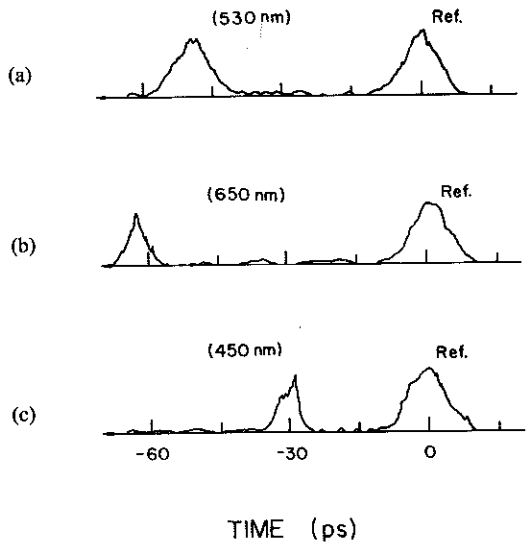

Fig. 4. Temporal profiles and pulse locations of a selected 10 nm band of a supercontinuum pulse at different wavelengths propagating through a 20 cm long CCl_4 cell. (a) $\lambda = 530$ nm. (b) 650 nm. (c) 450 nm. Amplitudes of these pulses are adjusted for display. The time zero is set for a reference pulse traveling in air. Filter effects were compensated. Different wavelengths were selected using narrow-band filters of the same thickness.

lated from the group velocity dispersion of a 10 nm band at the 650 nm supercontinuum traveling over 20 cm of liquid CCl_4 is negligible in our case.

C. SPM Signal Enhancement in Saltwater

Recently, we measured supercontinua that were several times larger in saline than in pure water. Relative to pure water, optical Kerr effect signals from saturated aqueous solutions of $ZnCl_2$ are increased by ~ 35 times, and supercontinua from saturated aqueous solutions of K_2ZnCl_4 are increased ~ 10 times. Typical spectra of supercontinua on the Stokes side, for KCl, $ZnCl_2$, and K_2ZnCl_2 aqueous solutions and neat water, have shown a wideband SPM spectrum together with the SRS of the OH stretching vibration around 645 nm. The addition of salts causes the SRS signal to shift towards the longer wavelength region and sometimes to reduce the SRS intensity. The SRS signals of pure water and dilute solutions appear in the hydrogen-bonded OH stretching region (~ 3400 cm^{-1}). In a high-concentration solution, it appears in the non-hydrogen-bonded OH stretching region (~ 3600 cm^{-1}). This is the same phenomenon that was observed in an aqueous solution of $NaClO_4$ by Walrafen [50].

To evaluate quantitatively the effect of cations on supercontinuum generation, the supercontinuum signal intensities for various samples at a fixed wavelength were measured and compared. Fig. 5 shows the dependence of the supercontinuum (mainly from the SPM contribution) signal intensity on salt concentration for aqueous solutions of K_2ZnCl_4, $ZnCl_2$, and KCl at 570 nm [Fig. 5(a)] and 500 nm [Fig. 5(b)]. These data indicate that the supercontinuum pulse intensity was highly dependent on salt concentration, and both the Stokes and anti-Stokes sides

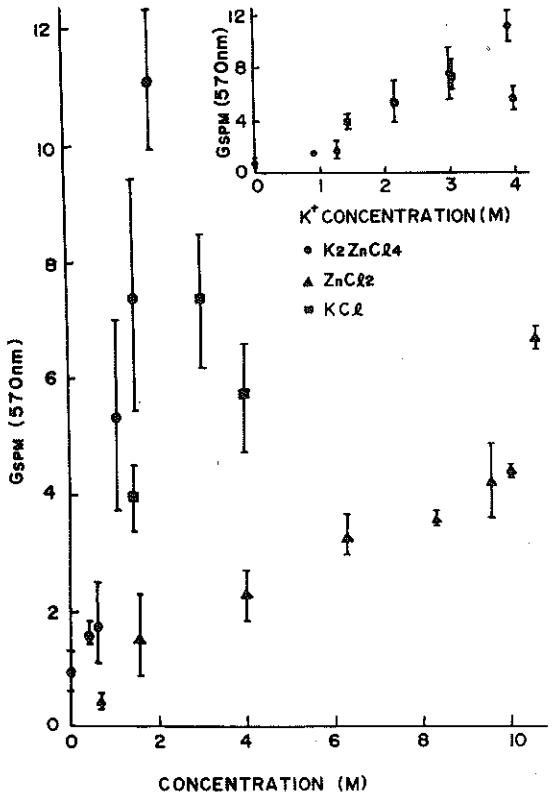

(a)

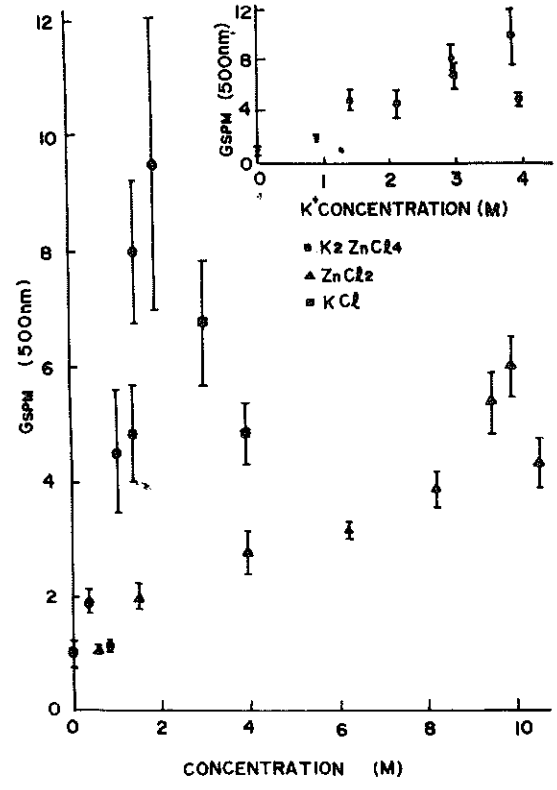

(b)

Fig. 5. Enhancement of continua in saltwater. (a) The salt concentration dependence of the SPM signal on the Stokes side at 20°C. (b) On the anti-Stokes side at 20°C. Each data point is the average of about ten laser shots. The insets are the same data plotted as a function of K^+ ion concentration for KCl and K_2ZnCl_4 aqueous solutions where N is Avogadro's number and M is the molar concentration in moles per liter.

of the supercontinua from a saturated K_2ZnCl_4 solution were about 10 times larger than from neat water. The insets in Fig. 5 are the same data plotted as a function of K^+ ion concentration for KCl and K_2ZnCl_4 aqueous solutions. Solutions of KCl and K_2ZnCl_4 generate almost the same amount of supercontinuum if the K^+ cation concentration is the same, even though they contain different amounts of Cl^- anions. This indicates that the Cl^- anion has little effect on the supercontinuum generation. The Zn^{2+} cation also enhanced the supercontinuum, although to a lesser extent than the K^+ cation.

The enhancement of the optical nonlinearity of water by the addition of cations can be explained by the cations' disruption of the tetrahedral hydrogen-bonded water structures and their formation of hydrated units [51]. Hydration increases as the number of water molecules per unit volume increases and thereby n_2 increases [52]. Furthermore, from the nonlinear distortion of the salt ions and the saltwater molecule interactions, the total optical nonlinearity of a mixture modeled from a generalized Langevin equation [53] is determined by the coupled interactions of solute–solute, solute–solvent, and solvent–solvent molecules.

IV. XPM

A newly observed nonlinear phase modulation process observed is XPM. This process was proposed by Gersten, Alfano, and Belic in 1980 [27]. An ~1 μJ 25 ps 532 nm laser pulse was coupled into a 10 m long single-mode optical fiber. The single-mode optical fiber was custom-made by Corning Glass Company to operate at visible wavelengths. The cutoff wavelength of the fiber is 462 nm, the core diameter is 2.5 μm, the cladding diameter is 79 μm, the refractive index difference is 0.24 percent, and the silica dispersion at 532 nm is $D(\lambda) = 0.66$. The output from the fiber was passed into a 1 m Jarrell-Ash spectrometer. The spectra of the output laser pulses were recorded by a PAR OMA2. The overall system resolution of the spectral measurement was 0.25 nm.

Four typical measured spectra of the laser pulse after propagating in 10 m of fiber with different incident pulse energies are displayed in Fig. 6. There are five salient features depicted in the four curves shown in Fig. 6. First, the output bandwidth of the incident wavelength (532 nm) increases as the incident pulse energy is increased. Second, the output peak amplitude of the incident 532 nm line is nearly a constant value when the incident pulse energy is above a threshold value. Third, both the amplitude and spectral bandwidth of the first Stokes output wavelength (544.5 nm) increase as a function of incident pulse energy. Fourth, the spectral shape of Raman emission is asymmetrical due to dispersion and walkoff during the generation process [46], [48], [49]. Fifth, and most important, the broadened spectral bandwidth of the Raman line is larger than that of the incident laser line, the ratios of the spectral width of the Raman line to that of the laser line being 2.85, 3.0, and 2.8, in Fig. 6(b), (c), and (d), respectively.

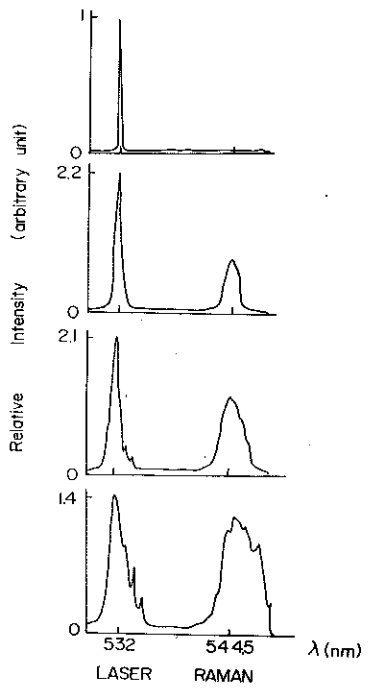

Fig. 6. Measured emission spectra of 25 ps laser pulses of different energies at a 532 nm wavelength propagating through a 10 m long single-mode glass fiber. The vertical axis is a relative intensity at the incident laser 532 nm wavelength. The horizontal axis is calibrated as a function of wavelength. The 544.5 nm corresponds to the peak of the first Stokes Raman line. (a) Relative pump pulse energy E_0. (b) Relative pump pulse energy $7E_0$. (c) Relative pump pulse energy $12E_0$. (d) Relative pump pulse energy $20E_0$.

From our previous theoretical analysis for XPM [27], the spectral bandwith of the Raman line should be increased as the pulses travel in the medium and grow dramatically as the pulse duration is shortened. The index of refraction of the system is of the form $n = n_0 + n_2E^2 + \gamma Q$ where γ determines the coupling of the phonon field Q to the electromagnetic field [27]. By assuming phase matching and neglecting group velocity dispersion and higher-order Raman processes, a coupled wave equation can be written as

$$\partial a_1/\partial n = i\left[\beta\left(|a_1|^2 + 2|a_2|^2\right)a_1 + \phi a_2\right], \quad (13a)$$

$$\partial a_2/\partial \eta = i\left[\beta\left(|a_2|^2 + 2|a_1|^2\right)a_2 + \phi^* a_2\right] \quad (13b)$$

where ϕ is proportional to the phonon amplitude and $\partial\phi/\partial\xi = -\phi + i\delta a_2^* a_1$; a_1 and a_2 denote the pulse envelope function of the incident laser and the first Raman Stokes, respectively; $\eta = \Gamma z/v$; $\xi = \Gamma(\tau - z/v)$; and Γ is the phonon decay rate. A predicted ratio of the Stokes spectral width to the primary spectral width without dispersion is [27]

$$X = \Delta\omega_{\text{Raman}}/\Delta\omega_{\text{laser}} = 2\left[1 + (\delta/2\beta)^2\right]^{0.5} \quad (14)$$

where

$$\beta = 3n_2\omega^3/(\Gamma n_0 c^2),$$

$$\delta = \gamma^2\omega^3/(16\pi\mu\sigma n_0 c^2\Gamma^2),$$

and ω is the incident laser frequency, σ is the phonon fre-

quency, μ is the effective oscillator mass density, n_0 is the linear index of refraction, and n_2 is the nonlinear index of refraction. Typical values for parameters in (14) are $\omega = 3.54 \times 10^{15}\ s^{-1}$, $\sigma = 8.3 \times 10^{13}$, $\mu = 1$ (estimated), $\gamma = 10^6$ (estimated), $n_0 = 1.5$, $n_2 = 1.2 \times 10^{-13}$ esu, and $\Gamma = 5.7 \times 10^{12}\ s^{-1}$. In a glass fiber, $\delta/2\beta \ll 1$, the ratio $X = 2$. Our experimental data have demonstrated this CPM signature. The spectral broadening of the Raman line is larger than that of the laser line. The measured ratio of these spectral broadenings under our experimental conditions was 2.9 ± 0.1, which was larger than the predicted twofold increase. In our measurement, the Raman intensity was nearly at the same intensity as the incident pulse. Equation (14) is an approximation when $a_2 \ll a_1$. At high Raman intensity, SPM by the Raman pulse itself should be added to the denominator of (14) and will increase the broadening ratio.

It is interesting to note that in the absence of SPM and XPM processes, the bandwidth of the SRS from a picosecond or femtosecond pulse is generally narrower [45]. This narrowing is due to the gain of SRS from the incident laser spectral profile. Equation (14) indicates a dominant contribution of spectral broadening to the Raman line from XPM and SPM in the absence of significant Raman gain. A significant contribution to the spectral broadening of the Raman line requires a large gain factor $\delta/2\beta \sim 1$ and a high incident laser power to saturate the gain.

When the group velocity dispersion is introduced into the calculation, (13) will be modified [49] due to the walkoff between the pump and Raman pulses [28], [29]. The spectral broadening of the Stokes side will be larger than that of the anti-Stokes under normal dispersion. This is opposite to the spectrally broadened distribution generated from SPM.

V. IPM

An important process of phase modulation for coding communications is IPM. The analysis for the IPM [31], [32] of the weak probe electric field of the SH pulse in the presence of a strong primary pump pulse can be expressed by the total field as

$$E = E_0[ae^{i\alpha}e^{i(kz-wt)} + \kappa be^{i\beta}e^{2i(kz-wt)}] \quad (15)$$

where E_0 is the amplitude of the primary pulse, κ is the relative strength of the SH pulse signal to the primary signal, a and b are the pulse shape functions of the primary and the SH signal, and α and β are the phases of these two pulses, respectively. Assuming $\kappa \ll 1$ and knowing the pulse shape function a, then b, α, and β can be derived. Neglecting fast oscillatory terms in χ^3 and assuming the group velocity v to be constant for frequencies from 400 to 1060 nm in glass, the quasilinear partial differential equations deduced from the nonlinear Maxwell equation [32] are

$$\partial a/\partial V - 1.5\epsilon a^2 \partial a/\partial U = 0 \quad (16a)$$

$$\partial b/\partial V - 0.5\epsilon a^2 \partial b/\partial U = \epsilon ab\,\partial a/\partial U \quad (16b)$$

$$\partial a/\partial V - 0.5\epsilon a^2 \partial\alpha/\partial U = 0.5K\epsilon a^2 - 0.125K\epsilon^2 a^4 \quad (16c)$$

$$\partial\beta/\partial V - 0.5\epsilon a^2 \partial\beta/\partial U = K\epsilon a^2 - 0.25K\epsilon^2 a^4 \quad (16d)$$

where τ is the pulse duration, $K = w\tau$, $U = (z/v - t)/\tau$, $V = z/(v\tau)$, $\epsilon = n_2 E_0^2/n$, and n is the index of refraction. Given a proper envelope function a, the above partial differential equations can be solved to determine the induced pulse shape distortion b, and spectral broadening β, of the weak probe pulse. On assuming a sech pulse envelope function for the incident primary pulse, (15) can be rewritten to be

$$E = E_0[\text{sech } U \exp(iKU) + \kappa \text{ sech } (1.76U) \exp(2iKU)]. \quad (15a)$$

The induced shape of the weak probe SH pulse due to the presence of an intense primary pulse at various incident intensity levels $|E_0|^2$ is given in [32]. The frequency extent of IPM can be obtained from (16d) as a function of the incident pump laser intensity. Calculated [32] induced Stokes and anti-Stokes spectral extents for a weak SH pulse are displayed in Fig. 7.

Experimental results of the spectral distribution of induced ultrashort supercontinuum pulses and ultrashort supercontinuum pulses are displayed in Fig. 8. The average increase of the induced supercontinuum in a BK-7 glass from 410 to 660 nm is about 11 times the supercontinuum. In this instance, both the 527 and 1054 nm laser pulse energies were maintained to be nearly constant: 80 μJ for 527 nm and 2 mJ for 1054 nm. In this experiment, the 527 nm laser pulse generated a weak supercontinuum, and the intense 1054 nm laser pulse served as a catalyst to enhance the supercontinuum in the 527 nm pulse. The supercontinuum generated by the 1054 nm pulse alone in this spectral region was less than 1 percent of the total induced supercontinuum. The spectral shapes of the supercontinuum and induced supercontinuum in Fig. 8 have a similar spectral distribution when the 527 nm pulse energy is set at 80 ± 15 μJ.

Since the supercontinuum generation can be due to either the phase modulation and/or FPPG processes [1], it is important to distinguish between these two different contributions to the induced supercontinuum. Spatial filtering of the signal was used to separate the two main contributions. The induced supercontinuum spectrum shows a spatial spectral distribution similar to that of the conventional supercontinuum [1]. The collinear profile, which is due to the phase modulation, has nearly the same spatial distribution as the incident laser pulse. As mentioned before, two emission wings at noncollinear angles correspond to the FPPG supercontinuum arising from the phase-matching condition of the generated wavelengths emitted at different angles from the incident laser beam direction [1]. Using a photomultiplier system and spatial filtering, quantitative measurements of spectral contributions of the induced supercontinuum from the collinear

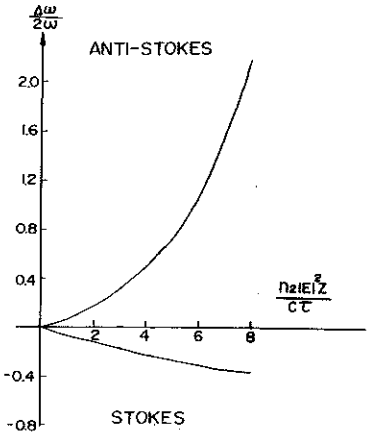

Fig. 7. IPM spectral extents as a function of the incident primary laser intensity. The horizontal axis $n_2 |E|^2 z/(c\tau)$ is a function of incident laser energy, and the vertical axis is the ratio of the frequency spread to SH. The incident second harmonic pulse energy is a constant. The asymmetry of the Stokes and anti-Stokes radiation has been observed experimentally.

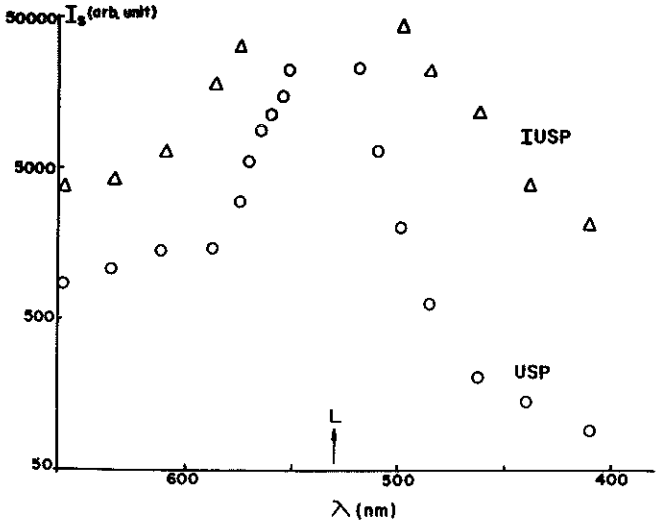

Fig. 8. Experimental induced supercontinuum intensity distribution from a BK-7 glass as a function of wavelength. Each data point was an average of about 20 laser shots and corrected from the detector, filter, and spectrometer spectral sensitivity. △ is the induced supercontinuum (IUSP) from both 530 and 1060 nm; ○ is the supercontinuum (USP) from 530 nm. The error bar of each data point is about ±20 percent. The supercontinuum from 1060 nm, which is not shown here, was ~1 percent of the induced supercontinuum.

IPM and the noncollinear FPPG parts were obtained [31]. These signals, measured at $\lambda = 570$ nm from the collinear and noncollinear parts of the induced supercontinuum, are plotted as a function of the pump pulse energy. There was little gain from the contribution of the FPPG process over the entire added pulse energy dependent measurement. The main enhancement process of the induced supercontinuum generation is consequently attributed to the IPM mechanism, which corresponds to the collinear geometry. This is a signature of IPM.

The discrepancy of the spectral distribution between the theoretical calculated curve of Fig. 7 and the experimental curve of Fig. 8 may be accounted for by the group velocity dispersion, which was neglected in the theory displayed in Fig. 7. The wider spread over the anti-Stokes spectral broadening is accounted for by the pulse-shape steepening. Due to the walkoff of the IPM in a normal dispersed medium, the broadening over the anti-Stokes side will be reduced. This is a reason why the experimental ratio of anti-Stokes broadening to Stokes broadening is less than the theoretical ratio.

Besides the two differences between XPM and IPM stated in Section I, an additional difference has been observed by comparing their spectral distributions. The asymmetric spectral shape of XPM has been observed to be more broadened on the Stokes side, while the asymmetric spectral shape of IPM is wider on the anti-Stokes side due to a shorter interaction length in a nonguided sample, and the probing wavelength of IPM is shorter than the pump wavelength.

VI. ISB

When an intense laser pulse propagates through noncentrosymmetric ZnSe crystals where both χ^2 and χ^3 are operative, ISB $> \pm 1000$ cm^{-1} around the non-phase-matched SH frequency can be produced [33]. The spectral broadening originates from the coupling of the third-order optical nonlinearity of ZnSe with the original intense 1054 nm picosecond laser pulse. The dominant mechanisms for ISB could be IPM, XPM, and the modulated two-photon excitonic polariton.

The following model is used to explain the general features observed for ISB of a weak SH pulse generated by an intense laser pulse in a medium with large second and third-order optical nonlinearities. The incident electric field at w_0 can be assumed to be

$$E(t) = E_0 \exp(-t^2/\tau^2) \cos[w_0 t + \phi(t)] \quad (18)$$

where E_0 is the amplitude of the primary wave and $\phi(t)$ is the phase term of the incident field propagating in ZnSe. The phase behaves as

$$\begin{aligned}\phi(t) = nzw_0/c \sim z_0 w_0/c[n_0 &+ n_1 E_0 \\ &\cdot \exp(-t^2/\tau^2) \cos(w_0 t - n_0 w_0 z_0/c) \\ &+ n_2 E_2^2 \exp(-2t^2/\tau^2) \\ &\cdot \cos^2(w_0 t - n_0 w_0 z_0/c) + \cdots]. \end{aligned} \quad (19)$$

For a thin medium and neglecting dispersion, (19) can be substituted into (18) to yield the total field as

$$\begin{aligned}E(t) = E_0 \exp(-t^2/\tau^2) &\cdot [A \cos(w_0 t - \Omega - \alpha_2) \\ &+ B \cos(w_0 t - \Omega + \alpha_2) \\ &+ C \sin(w_0 t - \Omega - \alpha_2) \\ &+ D \sin(w_0 t - \Omega + \alpha_2) \\ &+ E \cos(2w_0 t - 2\Omega - \alpha_2) \\ &+ F \cos(2w_0 t - 2\Omega + \alpha_2) \\ &+ G \sin(2w_0 t - 2\Omega - \alpha_2) \\ &+ H \sin(2w_0 t - 2\Omega + \alpha_2)] \end{aligned} \quad (20)$$

where

$$\Omega = n_0 w_0 z_0 / c,$$

$$\alpha_1 = (1/c) n_1 w_0 z_0 E_0 \exp(-t^2/\tau^2)$$

$$\alpha_2 = (1/2c) n_2 w_0 z_0 E_0^2 \exp(-2t^2/\tau^2)$$

are induced parameters and A, B, C, $\cdots$ are Taylor's series expanded Bessels functions with arguments α_1 and α_2 as

$$A = J_0(\alpha_1) J_0(\alpha_2) + \sum_{m=1}^{\infty} (-1)^m J_{4m}(\alpha_1) J_{2m}(\alpha_2);$$

$$B = -J_0(\alpha_1) J_0(\alpha_2) + \sum_{m=1}^{\infty} (-1)^{m+1} J_{4m+2}(\alpha_1) J_{2m}(\alpha_2);$$

$$C = J_2(\alpha_1) J_1(\alpha_2);$$

$$D = J_0(\alpha_1) J_1(\alpha_2) + \sum_{m=1}^{\infty} (-1)^{m+1} J_{4m}(\alpha_1) J_{2m-1}(\alpha_2); \text{ etc.}$$

$E(\omega)$ can be obtained by using the Fourier analysis (20). In (20), one can clearly identify the ISB ($2w_0 \pm \partial\alpha_2/\partial t$) term around the SH frequency $2w_0$ due to the primary laser intensity E^2, while regular SPM arises from $w_0 \pm \partial\alpha_2/\partial t$ terms. Numerical calculations using a coupled nonlinear equation similar to (20) in conjunction with the Fourier transformation are being pursued to obtain spectral information on ISB. Qualitatively, (20) explains the observed spectral extent of the induced broadening as a function of incident pulse energy, crystal length, and n_2 in the following section.

A. Spectral Measurement of ISB

An 8 ps 2 mJ 1054 nm laser pulse was weakly focused into the ZnSe sample. The spot size at the sample was about 1.5 mm in diameter. The SH produced in ZnSe samples was about 10 nJ. The incident laser energy was controlled by changing the neutral density filters. The output signal was sent through a 0.5 m Jarrell-Ash spectrograph to measure the spectral distribution of the signal light using polaroid films and optical multichannel analyzers. The 1054 nm incident laser beam was filtered.

The spectral was measured using photographic films and OMA for non-phase-matching SHG and ISB generated in a 22 mm long ZnSe crystal by a 2 mJ 1054 nm laser pulse. The spectra from ZnSe and quartz samples are displayed in Fig. 9. The salient features of the ZnSe spectra indicate that the extent of the spectral broadening about the SH line at 527 nm depends on the intensity of the incident 1054 nm laser pulse. When the incident laser pulse energy was 2 mJ, there was significant spectral broadening of about 1100 cm^{-1} on the Stokes side and 770 cm^{-1} on the anti-Stokes side. There was no significant difference in the spectral broadening distribution measured in the single crystal and polycrystalline material. When the incident pulse energy was less than 1 mJ, the spectral broadening was found to depend monotonically on the pulse energy of the 1060 nm beam.

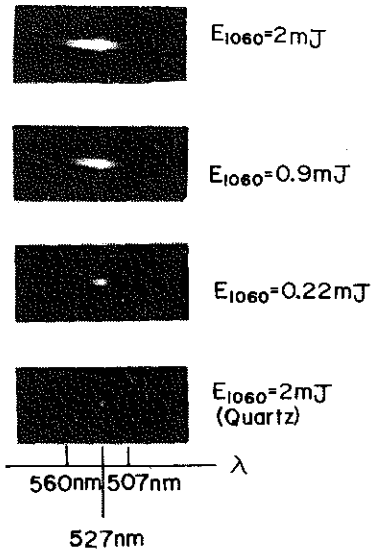

Fig. 9. ISB spectrum in a 22 mm long ZnSe excited by a 2 mJ 1054 nm pulse measured by an optical multichannel analyzer.

The spectral broadening generated by sending an intense 80 μJ 527 nm 8 ps laser pulse alone through these ZnSe crystals was also measured to compare to the $\sim \pm 1000$ cm^{-1} ISB discussed above. The observed spectral broadening was only ~ 200 cm^{-1} when the pulse energy of 527 nm was over 0.2 mJ. This measurement suggests that the SPM process from the 10 nJ SHG pulse in ZnSe is insignificant compared to the observed ~ 1000 cm^{-1} of ISB.

The second-order nonlinearity Pockels coefficient r_{ijk} of ZnSe is about 2×10^{-12} m/V [54], and the value of the third-order nonlinearity n_2 obtained by us from the optical Kerr effect was found to be about half the value of $n_2(CS_2) = 2 \times 10^{-11}$ esu. The Pockels term of ZnSe is responsible for the sharp line ~ 100 cm^{-1} at the SHG frequency. This weak 527 nm SHG pulse travels through the crystal together with the intense primary 1054 nm laser pulse. Due to the large n_2 of ZnSe and the intense incident 1054 nm laser, the spectral width about the weak 527 nm pulse is broadened [33]. The intensity ratio of the ISB to the non-phase-matched SHG signals displayed in Fig. 9 was ~ 0.1 for a given 1054 nm pulse energy. This conversion efficiency is much larger than the intensity conversion ratio of $\sim 10^{-4}$ observed for the induced supercontinuum about the 527 nm pulse in a BK-7 glass by propagating an intense 2 mJ 1054 nm laser pulse and a weak 80 μJ 527 nm laser pulse simultaneously. By replacing the ZnSe with a quartz crystal, only a narrow line at 527 nm was measured, as shown in Fig. 9. This observation can be explained by the lower n_2 value of quartz, which is about 50 times smaller than n_2 of ZnSe. It follows that $\Delta\nu_{\text{quartz}}$ is 50 times narrower than $\Delta\nu_{\text{ZnSe}}$.

A comparison between the theoretical model of (20) and

the experimental data in Fig. 9 is consistent. The broadened spectral width was proportional to the incident laser power from 0.2 to 2 mJ, to the length of ZnSe from 2 to 22 mm, and n_2 (ZnSe is about 100 times greater than quartz).

B. Temporal Measurement of ISB

The setup for the measurement of the temporal profile and distribution of ISB for ZnSe is shown in Fig. 1. A weak 527 nm pulse passing through a fixed distance in air set the zero reference time of the streak camera. The second beam of the 1054 nm pump was sent through the ZnSe sample. The temporal profile and the propagation time of the signals were measured by a 2 ps resolution streak camera system. The absolute time for the ISB traveling through the sample was determined by the time separation between the first reference pulse beam and the ISB signals in the streak camera. A set of color filters and narrow-band filters was used after the sample to select particular signal wavelengths to be analyzed.

The measured temporal profile of pulses propagating through a 22 mm ZnSe polycrystalline sample is shown in Fig. 10. Without the sample, both 1054 and 527 nm laser pulses appeared at the reference zero time point. A time delay of about 179 ps was observed for 527 nm in Fig. 10(a) when a weak 3 nJ 527 nm pulse propagated through the 22 mm ZnSe. A pulse delay of ~ 119 ps at 1054 nm was observed in Fig. 10(b) when an intense 1054 nm pulse passed through the crystal. The salient features of these traces [Fig. 10(c) and (d)] indicated that all the ISB wavelengths are reemitted at nearly the same time as the incident 1054 pulse [Fig. 10(b)].

The temporal behavior of a selected 10 nm band 530 nm signal from the 1054 nm generated ISB is shown in Fig. 10(c). The pulse shape and the duration of this signal, shown in Fig. 10(c), are quite different from those of the 1054 nm pumping pulse [Fig. 10(b)] and the 527 nm calibration pulse [Fig. 10(a)]. A ~ 60 ps long emission tail (from 179 to 119 ps) is the result of the emission of SHG of the 1054 nm pulse at different locations inside the ZnSe. An additional sharp spike is located at 119 ps, which is coincident with the 1054 nm pulse propagation time. Fig. 10(d) displays the temporal profile of the ISB pulse at 550 nm using a 10 nm width narrow-band filter. *The location of the ISB signal appears at the same time it takes the 1054 nm incident pulse to pass through the crystal.* The duration of the 550 nm ISB signal is ~ 5 ps, which is about half that of the incident 1054 nm pulse duration. The ISB signal at 510 nm showed properties similar to those of the 550 nm pulse.

The difference in the propagation of a weak 527 nm and a 1054 nm pulse through ZnSe, shown in Fig. 10(a) and (b), can be accounted for by group velocity dispersion. The measured group refractive indexes of ZnSe obtained from data displayed in Fig. 10(a) and (b) are $n_{g,527} = 3.44$ and $n_{g,1054} = 2.62$, respectively. These values are in good agreement with the calculated values [54] from the wavelength dependence of the group index of refraction: $n_{g,527} = 3.36$ and $n_{g,1054} = 2.58$; therefore, dispersion can account for the propagation of different wavelength pulses through ZnSe. However, *a new model is needed to explain the propagation of new ISB pulses 500–570 nm generated from the 1054 nm pulse in the crystal,* which appears to have about the same propagation time as the 1054 nm pulse.

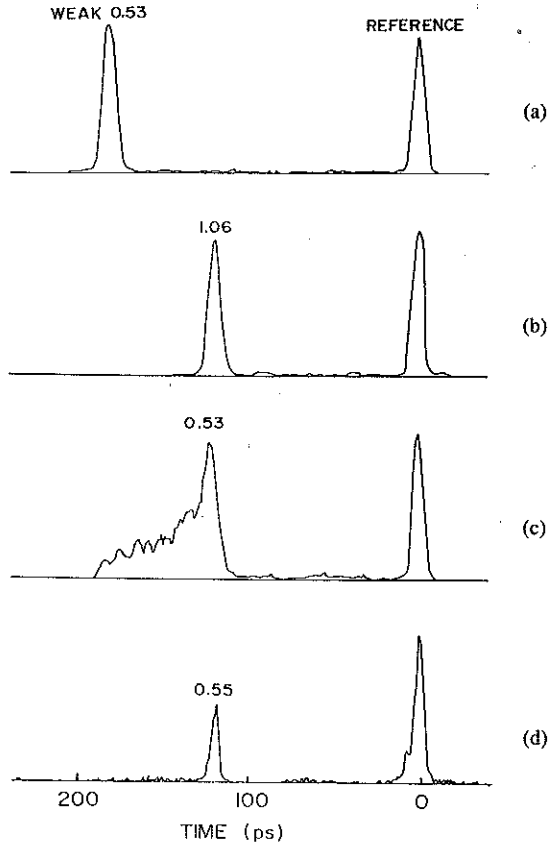

Fig. 10. Temporal profile and propagation delay times of ISB by a 22 mm long ZnSe crystal measured by a 2 ps resolution streak camera system. (a) Incident 527 nm. (b) Incident 1054 nm. (c) Generated 530 nm. (d) Generated 550 nm. The zero reference time corresponds to the laser pulse traveling through air without the crystal. This leads to a 73 ps time shift between the time scale here and the text. The right-hand side of the time scale is the leading time. The vertical scale is an arbitrary intensity scale.

There are several possible machanisms which may account for the observed dispersionless propagation of the ISB pulse relative to the incident 1054 nm pulse. One possibility is the compensation of the group velocity dispersion in ZnSe by the negative nonlinear index of refraction [55]–[58]. There are several negative nonlinear refractive index processes. These are the dynamic Burstein–Moss effect [55], induced free-carrier plasma [55], direct saturation of interband excitation [56], near-resonance pulse propagation [57], near excitonic molecule resonance [55], and spatial dispersion [59]. Our measured n_2 of ZnSe from picosecond OKE is about 10^{-11} esu. The laser power density needed to achieve the induced refractive index change to compensate the group index of $\delta n = n_{1054} - n_{527} \sim -0.8$ is TW/cm^2. This power density can be achieved using a 1 mJ 8 ps laser pulse with a beam diameter of ~ 40 μm. However, based on this model, the delay time

of the ISB should be sensitive to the 1054 nm power density (incident energy). This is not apparent in our measurements. In addition, theoretical calculations of δn from the above physical processes are orders of magnitude smaller than the required $\delta n = -0.8$. Therefore, this mechanism is questionable.

Another possible mechanism to explain the observed phenomena could arise from the enhanced SHG of the SPM process of 1054 nm. In this process, an intense 1054 nm pulse entering into the ZnSe is spectrally broadened from 1000 to 1140 nm due to SPM. The SHG of this 1054 nm SPM at the exit crystal surface may be larger than that in the bulk ZnSe. The surface-enhanced SHG process may arise from the surface roughness or the band distortion at the crystal surface. Therefore, a larger conversion of SHG (500–570 nm) may be possible at the exit crystal surface. However, there were four observations which contradicted this model. First, the measured intensity distribution of ISB from 500 to 570 nm is linearly proportional to that of SPM from 1000 to 1140 nm. Second, the output intensity ratio of the ISB was found to be linearly dependent on the sample thickness. Third, placing ZnSe in ethylene glycol or CS_2, to reduce the index mismatch between the crystal and air, made no difference in the output intensity on the time dynamics of ISB. Fourth, by changing the surface roughness of several ZnSe crystals with similar length and optical properties, the ISB intensity signal remained about the same.

The third possible model is the two-photon-like excitonic polariton. When an intense 1054 nm laser pulse enters a ZnSe crystal, two-photon excitation [60] is possible. Due to momentum conservation, the polarization dispersion curve of a two-photon excitation mode cannot follow the one-photon excitonic polariton dispersion curve. In the two-photon excitation process, the first photon ω_{1054} follows the original polariton curve. The second photon ω_{1054} starts with the same excitation process on the polariton curve [61] from the point $(\omega_{1054}, k_{1054})$ to the point $(2\omega_{1054}, 2k_{1054})$ where $2k_{1054} = 2\,(2\pi/\lambda_{1054})n_{1054}$. When a single photon ω_{527} is incident on ZnSe, the excitation mode will follow the solid curve and reach the point (ω_{527}, k_{527}) where $k_{527} = (2\pi/\lambda)n_{527}$. These two excitation modes, $(2\omega_{1054}, 2k_{1054})$ and (ω_{527}, k_{527}), have the same energy, but different momenta and slopes. The group velocity of the two-photon excitation mode is about the same as that of the ω_{1054} excitation mode, which is much larger than that of the ω_{527} excitation mode. However, in a temperature-dependent measurement of the strength of ISB from 4 to 300 K the output ISB intensity remained the same. This suggests a possibility of electronic generation such as SHG instead of polaritons where coupling is increased at low temperature.

A possible model to explain our unusual observation arises from the destructive interference of the non-phase-matched wavelength generation throughout the bulk material. Using the equation of the SHG [62] for a slowly varying time and space envelope function where second-order derivatives of the wave equation are neglected and the pump laser intensity is assumed to be constant, the SH envelope field can be expressed by [62]

$$E_{2,0}(t - z/v_2) = i\omega c\chi^2 \int_0^z E_{1,0}^2\left\{\left[t - z/v_2 - z'(1/v_1 - 1/v_2)\right]\right\} \cdot \exp - i(k_2 - 2k_1)z'\,dz' \quad (21)$$

where $E_{2,0}$ is the electric field envelope amplitude of SH at 2ω, v_1, and v_2 are group velocities for ω and 2ω, respectively, and k_1 and k_2 are wave vectors for ω and 2ω, respectively. The direct time-dependent experiments measured $E_{2,0}^2(t - z/v_2)$ generated in ZnSe crystal where the length of the crystal $z = L = 22$ mm for polycrystalline and 16 mm for the single crystal. The time t is the only variable in (21) after integration determined by the streak camera. The envelope function of the 1054 nm pump laser pulse has been measured to be a Gaussian function with $\tau_1 = 6/\sqrt{2 \ln 2}$ ps. Since $E_{1,0}^2$ is an even function and $\exp - i(k_2 - 2k_1)z'$ is a sinusoidal function, when $k_2 - 2k_1$ is nonzero for a non-phase-matched condition, the SHG emitted at the crystal exit surface at time t is an integrated solution of (21). For a given length $z = L$, if the phase factor $\exp -i(k_2 - 2k_1)z'$ oscillates over more than one period, the integration washes out, which results in $E_{2,0}$ becoming zero due to the summation of many SH pulses generated at different z' with + and − phases. This arises from destructive interference. Only at the entrance and exit parts of the crystal, part of the SHG pulses will not be canceled out from the free-space boundaries. As long as the group index difference and the crystal length are large enough that $(n_2 - n_1)L/c > \tau_1$, one should observe two separated peaks in time under the assumption of a nondepleted input and no absorption of the generated pulse. The peak separation will be $\Delta nL/c$.

In the experiment, the effective optical loss (absorption, collection, and scattering) of ZnSe at 527 nm gives $\alpha = 0.76\ \text{cm}^{-1}$. A modified calculation of (21) with the absorption loss at 2ω results in a reduction of the front surface signal [62]. This is one explanation why the measured SHG signal in Fig. 10(c) has only one peak from the exit surface. The other peak is absorbed. The plateau of SHG in Fig. 10(c) from 190 to 240 ps is not revealed in the first-order theoretical approximation shown in (21). This plateau may be accounted for by the nonnegligible group velocity dispersion. When the term $\tau^2/(\partial^2 k/\partial\omega^2)$ is comparable to the pulse interaction length, the second-order term $\partial^2 E_{2,0}/\partial t^2$ should be added to the approximated wave equation. Residues from nonperfect interference calculations can arise from a nonconstant Δk and nonmonochromatic laser pulses.

Including the χ^3 nonlinearity into P^{NL}, coupled-phase modulations similar to the IPM [31], [32] should occur to broaden the spectral width of the SH. Terms like $i\mu_0\omega c\chi^3 E_{1,0}^2 E_{2,0} \exp i[(k_2 - k_3)z - (\omega_2 - \omega_3)t]$ can be introduced into the approximated time-dependent wave equation for the ISB pulse in ZnSe at $\lambda = 500$–570 nm.

Similar solutions of the destructive cancellation, as shown in Fig. 10(c), can be obtained for the ISB pulses. That is what we have observed in Fig. 10(d); the 550 nm pulse was emitted at 187 ps. The difference between the missing wing or plateau of ISB in Fig. 10(d) compared to the SHG in Fig. 10(c) may arise from the ISB generation process. Destructive cancellation is more effective if Δk is constant and $\partial^2 k/\partial\omega^2$ is small.

The ISB and IPM processes appear similar. In both cases, the spectral width at 2ω was broadened by an intense pulse at ω. However, there are three differences. First, the 2ω pulse in ISB was internally generated in the coupled crystal. Second, the weak 2ω was generated in a non-phase-matched manner, which leads to destructive interference and a possible mechanism of the dispersionless-like propagation property. Third, so far ISB has only been observed in ZnSe where the internally generated 2ω pulse is near an absorption band with a large group velocity dispersion where the second-order differential term $\partial^2 k/\partial^2\omega$ may be responsible for part of the temporal properties displayed in Fig. 10(d).

VII. Summary

We have reviewed and identified several recently observed spectral broadening processes from picosecond and femtosecond laser pulses propagating in liquids, glasses, fibers, and semiconductors originating from SPM, XPM, IPM, and ISB. The latter three are closely related to each-other. The IPM and ISB of an ultrashort laser pulse have important features which could allow for pulse coding and possible dispersionless pulse propagation in different frequency regions. Knowledge of the spectral broadening mechanism as well as the capability of controlling the spectrum and pulse propagation may be useful in future optical communications, signal processing, squeeze states, and optical computation systems.

Acknowledgment

The authors thank their co-workers, S. L. Shapiro, W. Yu, J. Gersten, J. Zawadakas, N. Tzoar, P. Fleury, R. Seymour, J. Manassah, A. Katz, Q. Li, T. Jimbo, Q. Wang, and P. Baldeck for collaborating with them over the past 17 years. They also thank A. Johnson of BTL for helpful comments and N. Ockman for proofreading.

References

[1] R. R. Alfano and S. L. Shapiro, "Emission in the region 4000–7000 A via four-photon coupling in glass," *Phys. Rev. Lett.*, vol. 24, pp. 584–587, 1970; "Observation of self-phase modulation and small scale filaments in crystals and glasses," *Phys. Rev. Lett.*, vol. 24, pp. 592–594, 1970; "Direct distortion of electronic clouds of rare-gas atoms in intense electric fields," *Phys. Rev. Lett.*, vol. 24, pp. 1219–1222, 1970.

[2] J. Manassah, M. Mustafa, R. Alfano, and P. Ho, "Spectral extent and pulse shape of the supercontinuum for ultrashort laser pulse," *IEEE J. Quantum Electron.*, vol. QE-22, pp. 197–204, 1986.

[3] T. K. Gustafson, J. P. Taran, H. A. Haus, J. R. Lifsitz, and P. L. Kelley, "Self-modulation, self-steepening, and spectral development of light in small-scale trapped filaments," *Phys. Rev.*, vol. 177, pp. 306–313, 1969.

[4] F. Yablonovitch and N. Bloembergen, "Avalanche ionization of the limiting diameter of filaments induced by light pulses in transparent media," *Phys. Rev. Lett.*, vol. 29, pp. 907–910, 1972.

[5] R. A. Fisher and W. Bischel, "Numerical studies of the interplay between self-phase-modulation and the dispersion for intense plane wave laser pulse," *J. Appl. Phys.*, vol. 46, pp. 4921–4934, 1975.

[6] G. Yang and Y. R. Shen, "Spectral broadening of ultrashort pulses in a nonlinear medium," *Opt. Lett.*, vol. 9, pp. 510–512, 1984.

[7] N. Bloembergen and P. Lallemand, "Complex intensity dependent index of refraction frequency broadening of stimulated Raman lines and stimulated Rayleigh scattering," *Phys. Rev. Lett.*, vol. 16, pp. 81–84, 1966.

[8] F. Shimizu, "Frequency broadening in liquids by a short light pulse," *Phys. Rev. Lett.*, vol. 19, pp. 1097–1100, 1967.

[9] R. G. Brewer, "Frequency shifts in self-focused light," *Phys. Rev. Lett.*, vol 19, pp. 8–10, 1967.

[10] V. Kozobkin, A. Malyntin, and A. Prokhorov, "Phase self-modulation of Nd:glass laser radiation with mode-locking," *JETP Lett.*, vol. 12, pp. 150–152, 1970.

[11] R. Alfano, L. Hope, and S. Shapiro, "Electronic mechanism for production of self-phase modulation," *Phys. Rev. A*, vol. 6, pp. 433–438, 1982.

[12] R. Alfano, J. Gersten, G. Zawadzkas, and N. Tzoar, "Self-phase-modulation near the electronic resonances of a crystal," *Phys. Rev. A*, vol. 10, pp. 698–708, 1974.

[13] R. Alfano, P. Ho, P. Fleury, and H. Guggeneheim, "Nonlinear optical effects in antiferromagnetic $KniF_3$," *Opt. Commun.*, vol. 19, pp. 261–264, 1976.

[14] P. Corkum, P. Ho, R. Alfano, and J. Manassah, "Generation of infrared supercontinuum covering 3–14-μ in dielectrics and semiconductors," *Opt. Lett.*, vol. 10, pp. 624–626, 1985.

[15] R. Stolen and C. Lin, "Self-phase modulation in silica optical fibers," *Phys. Rev. A*, vol. 17, pp. 1448–1453, 1978.

[16] T. K. Gustafson, J. Taran, P. Kelley, and R. Chiao, "Self-modulation of picosecond pulse in electro-optical crystals," *Opt. Commun.*, vol. 2, pp. 17–21, 1970.

[17] J. Heritage, A. Weiner, and P. Thurston, "Picosecond pulse shaping by spectral phase and amplitude manipulation," *Opt. Lett.*, vol. 10, pp. 609–611, 1985.

[18] W. Knox, R. Fork, M. Downer, R. Stolen, and C. Shank, "Optical pulse compression to 8-fs at 5-KHz repetition rate," *Appl. Phys. Lett.*, vol. 46, pp. 1120–1121, 1985.

[19] N. Tzoar and M. Jain, "Self-phase modulation in long-geometry waveguides," *Phys. Rev. A*, vol. 23, pp. 1266–1270, 1981.

[20] D. Anderson and M. Lisak, "Nonlinear asymmetric self-phase modulation and self-steepening of pulses in long optical waveguides," *Phys. Rev. A*, vol. 27, pp. 1393–1398, 1983.

[21] L. Goldberg, "Broadband CARS probe using the picosecond continua," in *Ultrafast Phenomena III*. New York: Springer-Verlag, 1982, pp. 94–97.

[22] C. Shank, "Measurements of ultrafast phenomena in the femtosecond domain," *Science*, vol. 219, pp. 1027–1030, 1983.

[23] Y. Ishida, K. Naganuma, T. Yagima, and C. Lin, "Ultrafast self-phase modulation in a colliding pulse mode-locking ring dye laser," in *Ultrafast Phenomena IV*, D. H. Auston and K. B. Eisenthal, Eds. New York: Springer-Verlag, 1984, pp. 69–71.

[24] R. A. Fisher, B. Suydam, and D. Yevich, "Optical phase conjugation for time domain undoing of dispersion self-phase modulation effects," *Opt. Lett.*, vol. 8, pp. 611–613, 1983.

[25] P. B. Corkum, C. Rolland, and T. Rao, "Supercontinuum generation in gases," *Phys. Rev. Lett.*, vol. 57, pp. 2268–2271, 1986; J. Glownia, G. Arjavalingam, P. Sorokin, and J. Rothenberg, "Amplification of 350-fs pulses in XeCl excimer gain modules," *Opt. Lett.*, vol. 11, pp. 79–81, 1986.

[26] A. R. Chraplyvy, D. Marcuse, and P. S. Henry, *J. Lightwave Technol.*, vol. LT-2, p. 6, 1984; "Measurement of crossphase modulation in coherent wavelength-division multiplexing using injection lasers," *Electron. Lett.*, vol. 20, pp. 996–997, 1984.

[27] J. Gersten, R. Alfano, and M. Belic, "Combined stimulated Raman scattering and continuum self-phase-modulation," *Phys. Rev. A*, vol. 21, pp. 1222–1224, 1980.

[28] A. M. Johnson, R. H. Stolen, and W. M. Simpson, "The observation of chirped stimulated Raman scattered light in fibers," *Ultrafast Phenomena V*, G. R. Fleming and A. E. Siegman, Eds. New York: Springer-Verlag, 1986, pp. 160–163; R. H. Stolen and A. M. Johnson, "The effect of pulse walkoff on stimulated Raman scattering in fibers," *IEEE J. Quantum Electron.*, vol. QE-22, pp. 2154–2160, 1986.

[29] R. H. Stolen and J. E. Bjorkholm, "Parametric amplification and frequency conversion in fibers," *IEEE J. Quantum Electron.*, vol. QE-18, pp. 1072–1077, 1982; M. N. Islam, L. F. Mollenauer, R. H. Stolen, J. R. Simpson, and R. H. Shang, "Cross-phase modulation in optical fibers," *Opt. Lett.*, vol. 12, pp. 625–627, 1987.
[30] P. Cornelius and L. Harris, "Role of self-phase modulation in stimulated Raman scattering from more than one mode," *Opt. Lett.*, vol. 6, pp. 129–131, 1981.
[31] R. Alfano, Q. Li, T. Jimbo, J. Manassah, and P. Ho, "Induced spectral broadening of a weak picosecond pulse in glass produced by an intense ps pulse," *Opt. Lett.*, vol. 11, pp. 626–628, 1986.
[32] J. Manassah, M. Mustafa, R. Alfano, and P. Ho, "Induced supercontinuum and steepening of an ultrafast laser pulse," *Phys. Lett.*, vol. 113A, pp. 242–247, 1985.
[33] R. Alfano, Q. Wang, T. Jimbo, and P. Ho, "Induced spectral broadening about a second harmonic generated by an intense primary ultrashort laser pulse in ZnSe crystals," *Phys. Rev. A*, vol. 35, pp. 459–462, 1987.
[34] ——, "Dispersionless propagation of induced spectral broadened pulses in ZnSe," to be published.
[35] R. R. Alfano, "Ultrafast supercontinuum laser source," in *Proc. Int. Conf. Laser '85*, McLean, VA, Dec. 2–6, 1985, pp. 110–122.
[36] R. R. Alfano, Ed., *Biological Events Probed by Ultrafast Laser Spectroscopy*. New York: Academic, 1982; *Ultrafast Semiconductor Processes*, Vols. 1 and 2. New York: Academic, 1984.
[37] S. Shapiro, Ed., *Ultrashort Laser Pulses*. New York: Springer-Verlag, 1984.
[38] R. Fork, C. Shank, C. Hirliman, and R. Yen, "Femtosecond white light continua generation," *Opt. Lett.*, vol. 8, pp. 1–3, 1983.
[39] E. P. Ippen, C. V. Shank, and T. K. Gustafson, "Self-phase modulation of picosecond pulses in optical fibers," *Appl. Phys. Lett.*, vol. 33, pp. 1765–1767, 1974.
[40] M. Kitagawa and Y. Yamamato, "Number-phase minimum uncertainty state with reduced number uncertainty in a Kerr nonlinear interferometer," *Phys. Rev. A*, vol. 34, pp. 3974–3988, 1986.
[41] J. Manassah, P. Ho, A. Katz, and R. Alfano, "Ultrafast supercontinuum laser source," *Photon. Spectra*, pp. 53–59, Nov. 1984.
[42] L. M. Mollenauer, "The future of fiber communications: Solitons in all optical system," *Opt. News*, vol. 12, pp. 42–46, May 1986.
[43] P. P. Ho, A. Katz, R. R. Alfano, and N. Schiller, "Time-response of ultrafast streak camera system using femtosecond laser pulses," *Opt. Commun.*, vol. 54, pp. 57–62, 1985.
[44] Q. Li, T. Jimbo, P. P. Ho, R. Alfano, "Temporal distribution of ultrafast supercontinuum generated in a liquid measured by streak camera," *Appl. Opt.*, vol. 25, pp. 1869–1871, 1986.
[45] R. Alfano, "Interactions of picosecond pulses with matter," GTE, Bayside, NY, Tech. Rep. TR72-330.1, 1972.
[46] P. Ho, Q. Li, T. Jimbo, Y. Ku, and R. Alfano, "Supercontinuum generation and propagation in a liquid CCl_4," *Appl. Opt.*, vol. 26, pp. 2700–2702, 1987.
[47] H. Masuhara, H. Miyasaka, A. Karen, and N. Mataga, "Temporal characteristics of picosecond continuum as revealed by a two-dimensional analysis of streak images," *Opt. Commun.*, vol. 4, p. 426, 1983.
[48] G. P. Agrawal and M. J. Potasek, "Nonlinear pulse distortion in single-mode optical fibers at the zero-dispersion wavelength," *Phys. Rev. A*, vol. 33, pp. 1765–1776, 1986.
[49] D. Schadt, B. Jaskorzynska, and U. Osterberg, "Numerical study on combined stimulated Raman scattering and self-phase modulation in optical fibers influenced by walk-off between pump and Stokes pulses," *J. Opt. Soc. Amer.*, vol. B3, pp. 1257–1262, 1986; "Frequency chirp and spectra due to self-phase modulation and stimulated Raman scattering influenced by pulse walk-off in optical fibers," *J. Opt. Soc. Amer.*, vol. B4, pp. 856–862, 1987.
[50] G. E. Walrafen, "Stimulated Raman scattering and its mixture models in water," *Adv. Mol. Relaxation Processes*, vol. 3, pp. 43–49, 1972.
[51] ——, "Raman spectral studies of the effects of temperature on water and electrolyte solutions," *J. Chem. Phys.*, vol. 44, pp. 1546–1558, 1966.
[52] P. G. Klemens, "Anharmonic decay of phonons," *Phys. Rev.*, vol. 148, pp. 845–848, 1964.
[53] P. P. Ho and R. R. Alfano, "Coupled reorientational relaxation kinetics in mixed binary liquids directly measured by picosecond laser pulses," *J. Chem. Phys.*, vol. 68, pp. 4551–4562, 1978.
[54] H. H. Li, "Refractive indices of ZnS, ZnSe, and ZnTe and its wavelengths and ternary derivatives," *J. Phys. Chem. Ref. Data*, vol. 13, p. 103, 1984.
[55] D. A. B. Miller, S. D. Smith, and B. S. Wherrett, "The microscopic mechanism of third order optical nonlinearity in InSb," *Opt. Commun.*, vol. 35, pp. 221–226, 1980.
[56] S. Guha, E. Van Stryland, and M Soileau, "Self-defocusing in CdSe induced by charge carriers created by two-photon absorption," *Opt. Lett.*, vol. 10, pp. 285–287, 1985.
[57] M. D. Crisp, "Concept of group velocity in resonant pulse propagation," *Phys. Rev. A*, vol. 4, pp. 2104–2108, 1971.
[58] R. Baumert, I. Broser, and K. Buschick, "Nonlinearity of the refractive index due to an excitonic molecule resonance state in CdS," *IEEE J. Quantum Electron.*, vol. QE-22, pp. 1539–1542, 1986.
[59] A. Puri and J. L. Birman, "Pulse propagation in spatially dispersive media," *Phys. Rev. A*, vol. 7, pp. 1044–1052, 1983.
[60] E. Hanamura, "Giant two-photon absorption due to exciton molecules," *Solid-State Commun.*, vol. 12, p. 951, 1973.
[61] P. P. Ho and R. R. Alfano, "Induced modulation and induced spectral broadening," in *Proc. Int. Laser Conf., 86*, to be published.
[62] S. Akhmanov, A. Chirkin, K. Drabovich, A. Kovrigin, and A. Sukhorukov, "Nonstationary nonlinear optical effects and ultrashort light pulse formation," *IEEE J. Quantum Electron.*, vol. QE-4, pp. 598–605, 1968.

R. R. Alfano was born in New York, NY, on May 7, 1941. He received the B.S. and M.S. degrees from Fairleigh Dickinson University, Teaneck, NJ, in 1963 and 1964, respectively, and the Ph.D. degree in physics from New York University, New York, in 1972.

From 1964 to 1972 he was a member of the technical staff at GTE Research Laboratories, Bayside, NY, where he conducted studies on linear and nonlinear optical properties of materials and picosecond spectroscopy. Since 1972 he has been a professor with the Department of Physics, City College of New York, and in 1987 he became the Distinguished Professor of Science and Engineering. He is the Director of both the Institute for Ultrafast Spectroscopy and Lasers and the Photonic Engineering Laboratories.

Dr. Alfano is a Fellow of the American Physical Society and was an Alfred P. Sloan Fellow.

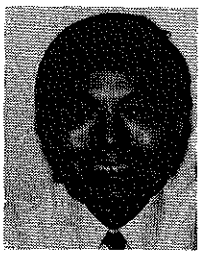

P. P. Ho was born in Taiwan in 1949. He received the B.S. degree from the National Tsing-Hua University, Taiwan, in 1970; the M.B.A. degree from Kent State University, Kent, OH, in 1983; and the Ph.D. degree from the City University of New York, New York, in 1978.

From 1973 to 1979 he was a graduate student and then a senior research associate at the Institute for Ultrafast Spectroscopy and Lasers, City College of New York, where he conducted studies of the picosecond Kerr effect, efficient energy transfer in dyes, and the development of femtosecond laser systems. From 1979 to 1983 he was a senior design engineer at the NCR Corporation and conducted research and development on an advanced laser scanning device. He is currently an associate professor of electrical engineering at the City College of New York.

Dr. Ho is a member of the American Physical Society and the Optical Society of America.